



Research paper

The film tells the story: Physical-chemical characteristics of IgG at the liquid–air interface

Ellen Koepf^{a,*}, Rudolf Schroeder^b, Gerald Brezesinski^c, Wolfgang Friess^a^aLudwig-Maximilians-Universität Munich, Department of Pharmacy, Pharmaceutical Technology and Biopharmaceutics, 81377 Munich, Germany^bAbbVie Deutschland GmbH & Co. KG, 67061 Ludwigshafen am Rhein, Germany^cMax Planck Institute of Colloids and Interfaces, Department of Biomolecular Systems, Potsdam-Golm Science Park, 14476 Potsdam, Germany

ARTICLE INFO

Article history:

Received 16 March 2017

Revised 15 May 2017

Accepted in revised form 13 July 2017

Available online 22 July 2017

Keywords:

Protein stability

Liquid–air interface

Interfacial film

Surface pressure

Surface spectroscopy

ABSTRACT

The presence of liquid–air interfaces in protein pharmaceuticals is known to negatively impact product stability. Nevertheless, the mechanisms behind interface-related protein aggregation are not yet fully understood. Little is known about the physical–chemical behavior of proteins adsorbed to the interface. Therefore, the combinatorial use of appropriate surface-sensitive analytical methods such as Langmuir trough experiments, Infrared Reflection-Absorption Spectroscopy (IRRAS), Brewster Angle Microscopy (BAM), and Atomic Force Microscopy (AFM) is highly expedient to uncover structures and events at the liquid–air interface directly. Concentration-dependent adsorption of a human immunoglobulin G (IgG) and characteristic surface-pressure/area isotherms substantiated the amphiphilic nature of the protein molecules as well as the formation of a compressible protein film at the liquid–air interface. Upon compression, the IgG molecules do not readily desorb but form a highly compressible interfacial film.

IRRAS spectra proved not only the presence of the protein at the interface, but also showed that the secondary structure does not change considerably during adsorption or compression. IRRAS experiments at different angles of incidence indicated that the film thickness and/or packing density increases upon compression. Furthermore, BAM images exposed the presence of a coherent but heterogeneous distribution of the protein at the interface. Topographical differences within the protein film after adsorption, compression and decompression were revealed using underwater AFM.

The combinatorial use of physical–chemical, spectroscopic and microscopic methods provided useful insights into the liquid–air interfacial protein behavior and revealed the formation of a continuous but inhomogeneous film of native-like protein molecules whose topographical appearance is affected by compressive forces.

© 2017 Elsevier B.V. All rights reserved.

1. Introduction

Protein pharmaceuticals are among the fastest growing and most important molecules in diagnostics and therapy, and therefore are of significant importance in high-impact areas such as autoimmune diseases and cancer [1]. The large size, the compositional variety and the distinct three-dimensional structure of protein molecules are causal for their sensitivity to undergo degradation processes.

Proteins undergo both chemical and physical degradation such as oxidation and hydrolysis, denaturation and aggregation [2]. Whereas a chemical instability reaction leads to a change in the primary structure of the protein, physical instability reactions result in a change of the spatial arrangement of the protein struc-

ture, without modification of covalent bonds. The immunogenic potential of protein pharmaceuticals is directly related to the emergence of aggregates [3]. So, the maintenance of the native conformation is essential for both the efficacy, as well as the safety of a protein drug [4–7].

Protein aggregation is highly undesirable due to the profound impact on the stability of the drug product, which can result in a loss of activity and unwanted immunogenic responses. In order to control protein aggregation, it is important to understand the underlying mechanisms. The fundamentals of protein aggregation were first described in the 1960s by the Lumry–Eyring model and are continually developed further [8–11].

Under physiological conditions, the three-dimensional structure of a protein represents an equilibrium between native and denatured (unfolded) states [8,12–14]. Exogenous influences during production, storage and transportation can lead to a shift in this balance. In the unfolded state, hydrophobic patches, usually

* Corresponding author.

E-mail address: ellen.koepf@googlegmail.com (E. Koepf).

buried in the core, can be exposed to the outside of the molecule, and therefore the denatured proteins are more prone to aggregation. The protein aggregates can be soluble or insoluble in nature, can be composed of covalent and non-covalent bonds, and can be reversible or irreversible [15]. Moreover, not only (partially) unfolded, but also native conformations are involved in the formation of aggregates [16]. In particular, the formation of so-called “large native-like” particles often occurs spontaneously, and no continuous pathway from monomer to dimer and then to large particles can be observed [10]. For instance, a self-association of native protein molecules has been reported for highly concentrated protein solutions as a result of macromolecular crowding-effects [17].

The propensity of protein molecules to accumulate and therefore concentrate at phase boundaries (e.g. solid–liquid, liquid–liquid, and liquid–air) plays an important role in several technological processes, for example during manufacturing and storage of protein pharmaceuticals. The migration of proteins from a bulk phase to an interface is similar to the adsorption process of small amphiphilic solutes, e.g. surfactants. A major distinction, however, is that a small surfactant molecule contains a defined hydrophilic head and hydrophobic tail that can easily partition towards the aqueous and non-aqueous regions of the interface, respectively. Such straightforward partitioning is not possible in the case of proteins. While most of the hydrophilic residues in the tertiary structure of proteins are exposed on the surface, not all hydrophobic residues are buried in the interior and some of them are exposed on the surface what finally imparts amphiphilicity to protein molecules [18]. Therefore, protein molecules adsorb to the liquid–air interface and thereby do not only lower interfacial tension but also form continuous gel-like films of highly concentrated protein via mainly non-covalent interactions [19,20]. The substantial differences in the surface activity of various proteins must be therefore related to their physical, chemical and conformational properties. Apart from intrinsic molecular factors, surface activity is also dictated by several extrinsic factors, such as pH, ionic strength, temperature or presence of other solution components such as sugars or surfactants. In addition to that, the molecular size of globular proteins affects their adsorption to the liquid–air interface [21,22].

Film formation and interfacial protein gelation have been identified as important triggers for the aggregation of protein pharmaceuticals [23–27]. For instance, adsorption of proteins to silicone oil, such as in prefilled syringes, can enhance protein aggregation [28]. Moreover, particle shedding from silicone tubings in peristaltic dosing pumps has to be considered [29]. Protein aggregation is also known to occur under different mechanical stress conditions, such as shaking [30,31]. Eliminating the liquid–air interface by removing the headspace in vials prevents agitation-induced aggregation as shown by Kiese et al. [32]. Furthermore, several studies suggest a clear connection between the disruption of the highly concentrated protein layer at the liquid–air interface and the occurrence of protein particles in the bulk solution [33,34]. Choosing appropriate formulation conditions, such as pH, ionic strength and additives (e.g. non-ionic surfactants), can stabilize proteins in pharmaceutical parenteral products against adsorption at surfaces and interface-induced aggregation [35–38].

In this study, different surface-sensitive analytical methods were applied for the characterization of important functional properties, such as adsorption, compressibility, as well as structural and topographical features of interfacial protein films. The combinational use of different physical–chemical methods enables comprehensive insights into the protein behavior at the interface. These new findings will not only help to understand how protein stability is affected by the events happening at the interface, but also to

identify and localize liquid–air interface related mechanisms of aggregation. Examination of particle formation by liquid–air interfacial stress only is not the subject of this study, but was addressed in separate investigations which are to be published soon.

2. Materials and methods

2.1. Materials

Human IgG (Beriglobin™, CSL Behring GmbH, Germany) was used for this study. The market product contains 159 mg/mL human IgG in 22 g/L Glycine and 3 g/L NaCl buffer at pH 6.8. Glycine-NaCl buffer was prepared using highly purified water (ELGA LC134, ELGA LabWater, Germany) and pH was adjusted adding NaOH. All diluted solutions were prepared by the addition of Glycine-NaCl buffer at pH 6.8 to the human IgG stock solution followed by filtration using 0.2 µm sterile PES filters (Sterile Syringe Filter PES, VWR, Germany).

2.2. Surface pressure measurements

Surface activity was expressed by surface pressure Π , with $\Pi = \sigma_0 - \sigma$, where σ_0 and σ are the aqueous subphase surface tension and the surface tension of the aqueous protein solution, respectively. Surface pressure measurements were performed in a $5.9 \times 39.7 \text{ cm}^2$ PTFE Langmuir trough equipped with a metal alloy dyne probe (Microtrough XS, Kibron Inc., Finland). For the determination of equilibrium surface pressures a 3×6 Multiwell Plate ($V = 0.8 \text{ mL}$) was used. Results are given as mean ($n = 3$) and standard deviation. Equilibrium adsorption pressure is defined as the maximum surface pressure that is reached by adsorption only and stable in a range of $\pm 0.2 \text{ mN/m}$ within 0.5 h.

160 mL sample solution was filled into the trough for the repeated compression-decompression measurements. The surface area of the trough can be varied by two movable PTFE barriers. Temperature was kept at 20 °C (K6-cc circulation thermostat, Peter Huber Kaeltemaschinenbau GmbH, Germany). Compression speed was set to 55 mm/min, and compression-decompression cycles were conducted from a maximum surface area of $A_{\text{max}} = 210 \text{ cm}^2$ to $A_{\text{min}} = 52 \text{ cm}^2$. Compression was started after the equilibrium adsorption pressure was reached.

2.3. FT-IR spectroscopy

For FT-IR measurements spectra were recorded using a Tensor 27 (Bruker Optics GmbH, Germany) connected to a thermostat (DC30-K20, Thermo Haake GmbH, Germany). For each measurement, the protein was formulated at 10 mg/mL in Glycine-NaCl buffer pH 6.8, and for each spectrum 100 absorbance scans were collected at a single beam mode with a resolution of 4 cm^{-1} . Spectra were analyzed by Opus 7.5 (Bruker Optics GmbH) and displayed as vector-normalized second-derivative spectra (calculated with 17 smoothing points according to the Savitzky-Golay algorithms [39]). Infrared spectra of the protein in solution were recorded using an AquaSpec (transmission cell H₂O A741-1) and BioATR (Attenuated Total Reflectance) cell™ II or BioATR (Attenuated Total Reflection), respectively, at 20 °C.

Infrared spectra of the temperature-induced unfolding of the IgG samples were conducted using the BioATR cell, as this sample cell can analyze protein samples either in solution or in suspension. Reference spectra were recorded under identical conditions with only the buffer (Glycine-NaCl buffer pH 6.8) in the cell. Temperature-dependent spectra were acquired every 4 °C from 25 to 93 °C with an equilibration time of 120 s. Recorded infrared spectra were analyzed by Protein Dynamics in Opus 7.5.

2.4. Infrared Reflection-Absorption Spectroscopy (IRRAS)

IRRAS was used to determine the presence and the conformation of the adsorbed protein at the soft liquid–air interface. IRRAS spectra were recorded using a VERTEX FT-IR spectrometer (Bruker Optics GmbH, Germany) equipped with a liquid nitrogen-cooled MCT (mercury cadmium telluride) detector. The spectrometer was coupled to a Langmuir trough (Riegler & Kirstein GmbH, Germany), placed in a sealed container (external air/water reflection unit XA-511) to guarantee constant vapor atmosphere. The IR beam was conducted out of the spectrometer and focused onto the water surface of the Langmuir trough. A computer controlled KRS-5 wire-grid polarizer (thallium bromide and iodide mixed crystal) was used to generate perpendicular (s) and parallel (p) polarized light. The angle of incidence was set to 40° with respect to the surface normal. Measurements were performed using a trough with two compartments and a trough shuttle system [40–42]. One compartment contained the protein solution under investigation (sample), and the other (reference) was filled with the pure buffer subphase. The single-beam reflectance spectrum (R_0) from the reference trough was taken as background for the single-beam reflectance spectrum (R) of the monolayer in the sample trough to calculate the reflection–absorption spectrum as $-\log(R/R_0)$ in order to eliminate the water vapor signal. IR spectra were collected at 8 cm^{-1} resolution and a scanner speed of 20 kHz. For s-polarized light, spectra were co-added over 200 scans, and spectra with p-polarized light were co-added over 400 scans. To distinguish between the influence of increasing concentration and changed orientation on the signal intensity, the dichroic ratio DR of the amide I band at 1643 cm^{-1} was calculated as $DR = A_p/A_s$, with A_s and A_p being the maximum absorption obtained with s-polarized light and p-polarized light, respectively.

For the determination of the interfacial film thickness in equilibrium and after compression to 30 mN/m, the incidence angle of the IR beam was varied with respect to the surface normal between 30° and 72° in steps of 2° or 3° . IRRAS spectra were simulated using a MATLAB program [43,44] on the basis of the optical model of Kuzmin and Mikhailov [45,46]. The intensity and shape of a reflection–absorption band depend on the absorption coefficient k , the full-width of half-height (fwhh), the orientation of the transition dipole moment (TDM) within the molecule α , the molecular tilt angle θ , the polarization and the angle of incidence (AoI) of the incoming light, as well as the layer thickness d and its refractive index n . Simulated spectra were fitted to the experimental data in a global fit, where all spectra recorded at different AoI and different polarizations were fitted in one non-linear least square minimization using the Levenberg-Marquardt algorithm. The polarizer quality was set to $\Gamma = 0.01$. The optical constants of the water subphase were taken from Bertie et al. [47,48]. The layer thickness d was determined from a fit of the OH stretching vibrational band ($\nu(\text{OH})$) in the range of $3800\text{--}3000\text{ cm}^{-1}$. Additional experimental details are described elsewhere [49–52].

2.5. Brewster Angle Microscopy (BAM)

The morphology of the monolayer was imaged with a Brewster angle microscope, BAM2plus from NanoFilm Technologie GmbH (Goettingen, Germany), equipped with a miniature film balance from NIMA Technology (Coventry, UK). IgG at 1 mg/mL in Glycine-NaCl buffer at pH 6.8 was filled into the trough ($V = 80\text{ mL}$). Simultaneous surface pressure measurements during adsorption and compression of the IgG in the Langmuir trough enabled a direct connection of each image with the corresponding surface pressure during adsorption or compression of the protein. The lateral resolution of the BAM was approximately $3\ \mu\text{m}$. The size of the

BAM images is $400 \times 720\ \mu\text{m}^2$. Detailed information about the BAM method is given elsewhere [53–55].

2.6. Atomic Force Microscopy (AFM)

For AFM, protein films formed during adsorption to equilibrium adsorption pressure or after compression to a desired surface pressure, were transferred by the Langmuir-Schaefer deposition (horizontal transfer of the film) using $1 \times 1\text{ cm}^2$ mica plates (Mica Sheet V5 Quality, Science Services GmbH, Germany) attached to a stamp tool. The mica was lowered onto the surface and pulled off after 2 s of contact time. The mica was removed from the stamp tool and the transferred film was covered with a drop of buffer solution to prevent drying of the sample. The transferred films were analyzed by underwater AFM (Bruker/Veeco/Digital Instruments MultiMode AFM) using a cantilever (Arrow™ NCPt, resonance frequency 285 kHz, spring constant 42 N/m) in tapping mode (Nano World AG, Switzerland). Images were analyzed by NanoScope III 5.12r3 Software (Digital Instruments Inc., US).

For the determination of interfacial film thickness, the film was transferred onto silica by Langmuir-Schaefer technique. A scratch was made using stainless steel tweezers. Film thickness was determined by section analysis from an average of 6 measuring points from the silica substrate to the film (area unaffected by the scratch).

3. Results and discussion

3.1. Time and concentration dependent adsorption of IgG

Surface pressure measurements were performed to investigate the adsorption kinetics of the IgG from bulk solution to the liquid–air interface. IgG reveals a pronounced surface activity as shown in Fig. 1a. IgG in a concentration 0.01 mg/mL reaches surface pressure values of 6.7 mN/m after 300 min, whereas IgG in a concentration of 0.5 mg/mL reaches an equilibrium surface pressure value of 18.2 mN/m after about 270 min. In case of a 1 mg/mL IgG solution, the equilibrium adsorption pressure is only slightly higher (18.5 mN/m after 240 min). Although the adsorption of globular proteins such as IgG starts immediately, equilibrium adsorption pressures are reached only after several hours and depend on the protein itself and on the formulation conditions [21,22,56]. Adsorption of small surfactants, such as polysorbate 20 or 80, is much faster, and equilibrium adsorption pressure values

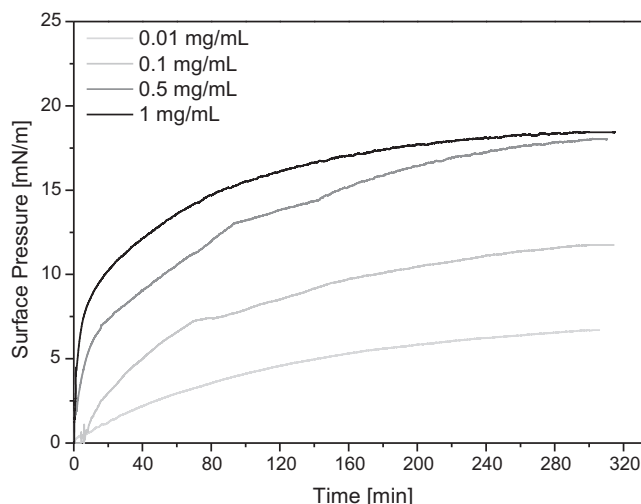


Fig. 1a. Time-dependent adsorption of IgG using different bulk concentrations.

are reached within less than 30 min due to the distinct amphiphilic character and the low molecular weight [18,36,57].

Fig. 1b shows the concentration-dependent equilibrium adsorption pressure using protein concentrations of 0.001 mg/mL up to 12 mg/mL IgG. At low IgG concentrations in the range from 0.01 mg/mL to 0.1 mg/mL, the concentration-dependent change in surface pressure is pronounced, whereas concentrations ≥ 1 mg/mL do not lead to any further considerable increase in equilibrium adsorption pressure. Therefore, for further experiments a concentration of 1 mg/mL was considered to be adequate. This correlation between protein concentration and equilibrium adsorption pressure can be interpreted in terms of the surface coverage [16,31]. At protein concentrations ≥ 1 mg/mL IgG, the protein molecules may form multilayers, but these structures do not contribute significantly to the surface pressure [58]. Moreover, a highly viscous protein film is formed, which can be deformed by lifting and lowering the dyne probe (Fig. 2) and is caused by mainly non-covalent interactions of the highly concentrated protein layer at the liquid–air interface [59,60].

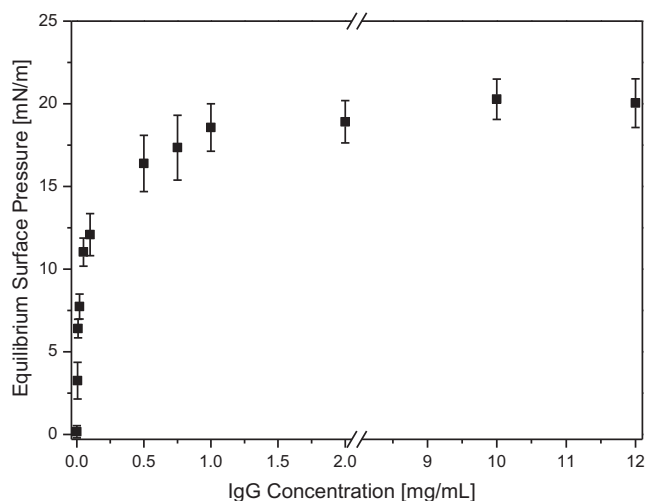


Fig. 1b. Concentration-dependent equilibrium adsorption pressure of IgG.

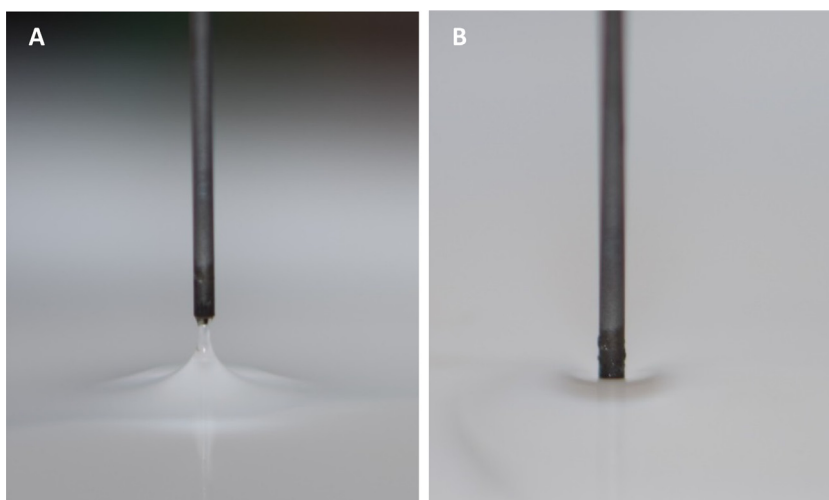


Fig. 2. IgG film at equilibrium adsorption pressure deformed by lifting (A) or lowering (B) the dyne probe.

3.2. Repeated compression-decompression of interfacial IgG films

Repeated compression-decompression was performed to investigate the physical resistance of the IgG film at the liquid–air interface. Controlled compression and decompression ensure that mechanical stress is applied to the interfacial IgG film only, while simultaneously the surface pressure is recorded. Movement of the barriers from maximum surface area (A_{\max}) towards the minimum surface area (A_{\min}) results in an increase in surface pressure from the equilibrium adsorption pressure of 18.5 mN/m up to 52 mN/m (Fig. 3). The change in surface pressure upon compression of the film is 33.5 mN/m after the first cycle and does not noticeably change with the following cycles. During the first compression, the slope between 210 cm² (A_{\max}) and 140 cm² is much lower compared to the slope of the isotherm between 120 cm² and 52 cm² (A_{\min}). This indicates a drastic change in compressibility of the protein film. Upon decompression, the surface pressure decreases strongly between 52 cm² and 70 cm², whereas the slope of the isotherm is low between 80 cm² and A_{\max} . Curve progression

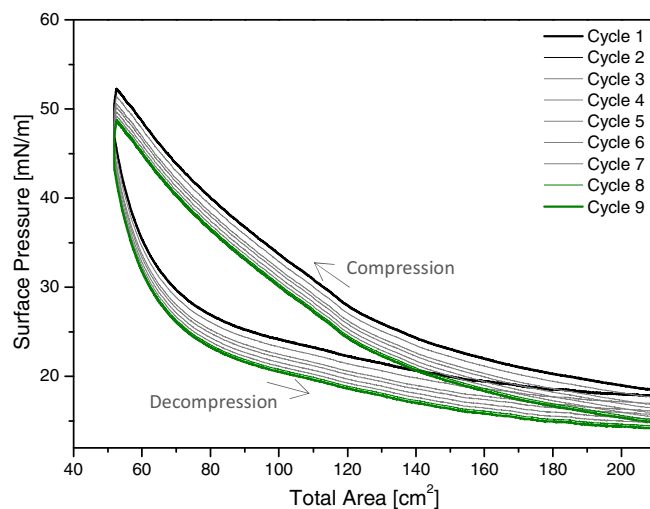


Fig. 3. Compression-decompression cycles of IgG in the Langmuir trough. Compression starts at A_{\max} at equilibrium (18.5 mN/m) adsorption pressure and ends at A_{\min} . Decompression starts at A_{\min} and ends at A_{\max} .

is nearly identical for each cycle with a slight decrease in the surface pressure at A_{\max} in each cycle. The compression of the film causes a compaction of the proteins connected with a decrease in molecular area modifying the ordering of the protein molecules and the distribution across the interface [61]. This can be connected with an increase in film thickness and/or changes in molecule orientation [62]. Moreover, the surface pressure increase demonstrates that the protein molecules stay at the interface upon compression. This non-equilibrium between adsorption and desorption can be traced back to the formation of a viscoelastic film where in addition to hydrophobic interactions, hydrogen bonds also contribute substantially to the molecular association [63].

The steep decrease in the initial stage of decompression (between 52 cm^2 (A_{\min}) and 70 cm^2) can be explained by a short-term rupture of the film followed by re-adsorption or re-spreading of protein molecules at the interface, ending in a quasi-equilibrium surface pressure when decompression is completed. Based on the decrease in surface pressure after each cycle compared to the initial value a loss of material from the interface can be assumed [33]. The high compressibility and the appearance of a considerable hysteresis between compression and decompression substantiate the formation of a viscous protein network at the interface which is in accordance with the film deformation as shown in Fig. 2. The hysteresis indicates that the protein does not desorb upon compression and that the interfacial film undergoes physical changes during compression and decompression [41–43].

3.3. Temperature-induced unfolding of IgG

To determine possible changes in the secondary structure, FT-IR spectra were recorded upon heating. The melting temperature (T_m) of IgG was identified to be $72 \text{ }^\circ\text{C}$ using microcalorimetry [64]. By increasing the temperature above T_m , changes in the secondary structure occurred indicated by changes in the amide I modes (Fig. 4). Starting the temperature ramp, IgG exhibited the amide I band maximum at 1639 cm^{-1} characteristic for intramolecular β -sheet structures. Additionally, bands with wavenumbers centering around 1620 cm^{-1} and 1690 cm^{-1} assignable to extended strands and to weak intramolecular β -sheet or turns, respectively, can be identified.

Elevation of the temperature resulted in the following spectral changes: the amide I absorbance maximum around 1639 cm^{-1} decreased accompanied by an intensity increase at 1625 cm^{-1} .

Additionally, a peak shift from 1690 cm^{-1} to 1695 cm^{-1} occurred representing a shift to intermolecular β -sheet structures. The loss of the native intramolecular β -sheet structure towards a more unordered structure with distinctive bands of intermolecular β -sheet structures (1625 cm^{-1} and 1695 cm^{-1}) is in accordance with the results obtained by Matheus et al. [65]. In addition to the formation of intermolecular antiparallel β -sheet structures indicated by peak shifts, the presence of new protein interactions after heating resulted in gel formation of the cooled samples, which is characteristic for extensive intermolecular interactions in protein samples [66].

3.4. Presence and secondary structure of IgG at the interface

The presence of the IgG at the liquid–air interface can be confirmed by IRRAS measurements. Furthermore, a comparative analysis of secondary structure elements of the IgG in solution and at the interface enables conclusions whether the adsorption to the interface and the compression of the adsorbed protein film cause conformational changes.

The appearance of the water band and the amide A, I and II bands prove the formation of an IgG adsorption layer at the interface. The amide I band is associated mostly with the C=O stretching vibration, and the amide II band results from in-plane NH-bending and CH-stretching vibrations. The amide A band is due to N–H stretching vibration. This vibrational mode does not depend on the backbone conformation but is very sensitive to the strength of hydrogen bonds. Wavenumbers between 3225 cm^{-1} and 3280 cm^{-1} have been found for hydrogen bond lengths between 2.69 \AA and 2.85 \AA [67]. The intensity of the bands increases during the adsorption process and also upon compression to surface pressure values above the equilibrium adsorption pressure (Figs. 5 and 6). The intensity of the OH-band around 3600 cm^{-1} is directly connected with the effective adsorption-layer thickness, because the intensity of the water band in the spectrum of the sample trough is reduced in comparison to the one from the reference trough since the protein adsorption layer replaces a water layer of the same thickness [68]. Therefore the increasing intensity of the bands refers to an increasing interfacial protein concentration, film thickness and/or packing density within the film [43,69]. These results are consistent with the surface pressure measurements, where compression caused a significant increase in surface pressure due to an interfacial compaction of protein material and/or change in molecule orientation.

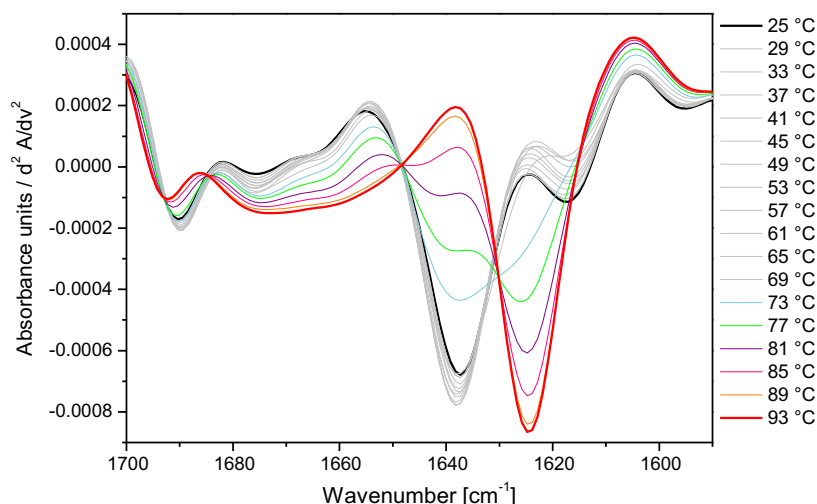


Fig. 4. Temperature-induced unfolding of IgG [10 mg/mL in Glycine-NaCl pH 6.8] between $25 \text{ }^\circ\text{C}$ and $93 \text{ }^\circ\text{C}$ in steps of $4 \text{ }^\circ\text{C}$ using FT-IR spectroscopy (BioATR).

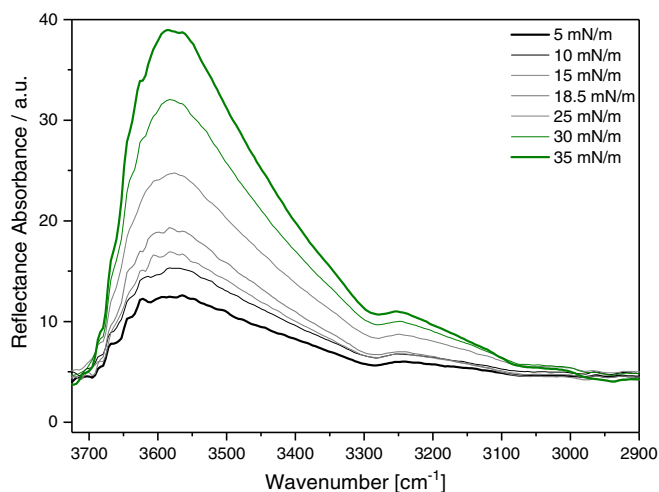


Fig. 5. IRRA spectra in the OH-stretching vibration region of IgG with increasing surface pressure (s-polarized light, $A_{ol} = 40^\circ$).

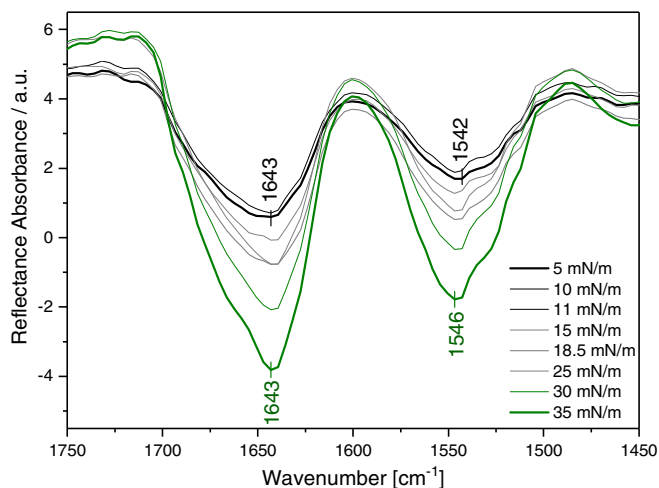


Fig. 6. IRRA spectra in the amid I and II regions of IgG with increasing surface pressure (s-polarized light, $A_{ol} = 40^\circ$).

With increasing surface pressure, the intensity of the amide bands increases. The maximum of the amide I band is observed at 1643 cm^{-1} and in the amide II region at $\sim 1543\text{ cm}^{-1}$ (Fig. 6). The IRRA spectra indicates an intramolecular β -sheet or unordered random coil conformation of the IgG at the interface [70]. The position of the amide I band does not change with increasing surface pressure indicating that the secondary structure of the adsorbed IgG changes neither during adsorption nor during compression.

Fig. 7 shows the FT-IR spectrum of the native IgG in solution using the AquaSpec and the BioATR measurement cell, respectively. The band positions of the transmission as well as of the attenuated total reflection (ATR) spectrum can be assigned to a mostly intramolecular β -sheet structure of the IgG in solution. Comparison of the two spectra reveals slight differences in the band positions with 1639 cm^{-1} for the AquaSpec, and 1636 cm^{-1} for the BioATR cell. This can be explained by the different measurement techniques as the AquaSpec records transmission spectra of the aqueous protein solution, and the BioATR measures reflectance spectra of a protein film at the silicon crystal. Nevertheless, both measurement principles lead to fairly identical structural elements for the IgG. The position of the bands determined in FT-IR spectra (1639 cm^{-1} or 1636 cm^{-1}) and IRRA spectra (1643 cm^{-1}) differs

only marginally. The peaks of the IRRA spectra are broader compared to the FT-IR peaks. This can be explained by the higher resolution of the FT-IR and/or can be due to a peak overlapping within the amide I region of the IRRA spectra, containing not only the band at 1639 cm^{-1} but additional bands beside the band at 1690 cm^{-1} , which is also present in the FT-IR spectrum, reflecting an intramolecular β -sheet structure.

Unlike the conformational changes of the IgG induced by heat stress (Fig. 4), where strong peak shifts from the native intramolecular β -sheet structure at 1639 cm^{-1} towards a more unordered structure with a distinctive band of intermolecular β -sheet structure at 1625 cm^{-1} were observed, the adsorption of the IgG to the interface does not induce considerable conformational changes. As no other peaks referring to new structural elements appear, the IgG predominantly retains its native structure during adsorption as well as during compression.

The increase in the intensity of the IRRA bands as well as the increase in surface pressure upon compression can be attributed to an increase in the adsorbed protein amount either due to an increase in film thickness or to changes in the molecule orientation allowing higher packing densities. In order to discriminate between those two effects, the dichroic ratio (DR) was calculated. In Fig. 8, the DR values at 1643 cm^{-1} are plotted as a function of

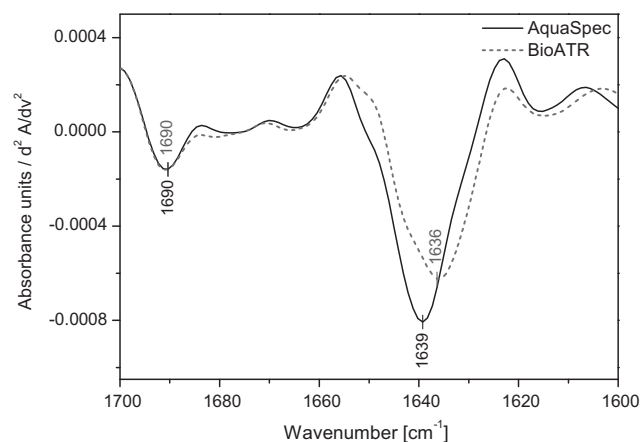


Fig. 7. Comparative FT-IR spectra of IgG in solution (AquaSpec vs. BioATR).

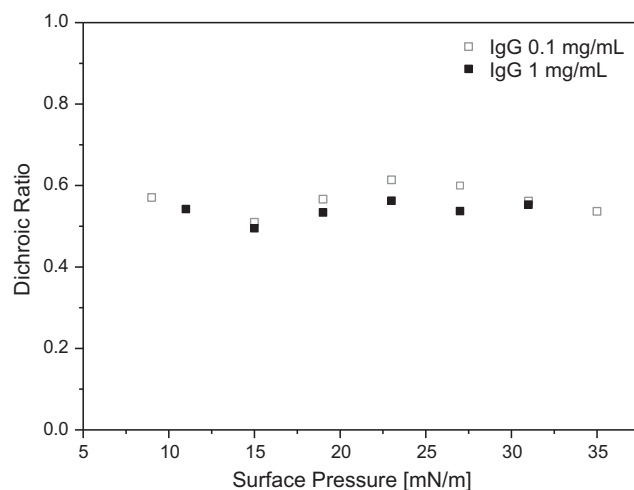


Fig. 8. Dichroic Ratio of amide I at 1643 cm^{-1} (p/s-polarized light, $A_{ol} = 40^\circ$) as a function of surface pressure at two different IgG concentrations.

surface pressure at two different IgG concentrations. No change in DR is observed during adsorption or compression, therefore the molecule orientation does not change with increasing surface pressure. Hence, the increase in surface pressure upon compression and the increase in the intensity of the IRRA bands can be solely explained by an increase in packing density and/or film thickness.

3.5. Structural and morphological characterization of the Liquid-Air interfacial film

BAM was used to visualize the liquid–air interfacial protein film. At the Brewster angle, p-polarized light is not reflected, and the bare buffer surface appears dark. In the case of protein adsorption, the Brewster condition is altered by the presence of the protein film with a different refractive index, indicated by an overall increased brightness as a part of the incident light is reflected (Fig. 9). Areas which appear dark in the BAM images are formed by a thinner but homogeneous film compared to brighter areas. Although the protein covers the entire interface, flickering domains are present immediately as adsorption starts representing differences in packing density. During adsorption, the surface appearance does not change. Moreover, even compression of the film does not affect the BAM images. Areas of increased brightness represent areas of increased packing density and film thickness [59,71]. The island-like structures demonstrate that the protein is not homogeneously distributed across the interface.

3.6. Changes in film topography caused by compression

Underwater Atomic Force Microscopy (AFM) was used to further elucidate the topographical properties of the interfacial protein film on a different scale compared to BAM. The film deposited after adsorption to equilibrium surface pressure confirms the presence of the IgG at the interface (Fig. 10A). Individual IgG molecules cannot be detected due to the flattening effect during AFM measurements in liquid medium [72]. Nevertheless, as in the BAM images, an inhomogeneous distribution of the protein after adsorption can be confirmed. Bright areas in the deflection image are considered to be protein material that protrudes above the protein layer with a height of 15 nm. The determined film roughness of 1.0 nm after adsorption is in accordance with literature values for other globular proteins [15,49].

Upon compression, areas of telescoped material appear (Fig. 10B) wherein the protein film forms wrinkles that protrude with a height of 18 nm from the remaining part of the compact film. A recent study by Ghazvini et al. [73] described similar findings for a dried film of an IgG₁ after compression. The presence of those areas of increased film thickness after compression can be explained as follows: compression first increases the packing density in the adsorption layer leading to an increase in surface pressure and the OH- and amide-bands intensities in the IRRA spectra. At high pressure, some material will be partially excluded from the well-packed film into the subphase during compression.

After decompression, the areas of telescoped material cannot be recognized any more (Fig. 10C). Thus, decompression leads to a steep decrease in surface pressure and results in a decrease of the overall height of the interfacial film. Additionally, a decrease in surface pressure after each compression–decompression cycle has been observed. This can be traced back to a loss of material from the interface [33,34,73].

3.7. Interfacial film thickness in equilibrium and after compression

Interfacial film thickness of the IgG film in equilibrium at 18.5 mN/m and after compression to 30 mN/m was determined by angle-dependent Infrared Reflection-Absorption Spectroscopy (IRRAS) measurements and compared to the values obtained by underwater AFM of the films after Langmuir-Schaefer transfer.

The increase in the intensity of the OH-stretching vibration around 3600 cm⁻¹ indicates an increase in effective film thickness upon compression. The two types of polarized light (s and p) have dramatically different reflectivity properties around the Brewster angle (~53.1°) with a minimized intensity of the reflected p-polarized light. As shown in Fig. 11, the reflectance-absorbance (RA) in the region of the OH-stretching vibration changes continuously for s-polarized light as a function of the angle of incidence (AoI), whereas RA of p-polarized light exhibits a discontinuity around the Brewster angle. The IRRA spectra taken with p- and s-polarized light have been compared with the corresponding simulated spectra with the OH-stretching vibration $\nu(\text{OH})$ and the amide A band (Fig. 11).

In Fig. 12, the maxima of the RA intensities of experimental and simulated spectra at different AoI have been compared. The best fit of the simulated to the experimental data allows the determination of the layer thickness, assuming a refractive index of the protein layer. The presented simulation is based on a refractive index (n) of the protein solution using experimental data. As the refractive index n of the protein solution directly depends on the concentration and packing density, it was set to 1.45 in the adsorption layer at equilibrium with a linearly increasing increment of 0.024 depending on the protein concentration. Therefore, the calculated interfacial film thickness after adsorption to an equilibrium surface pressure amounted to 1.97 nm and increases upon compression to 2.61 nm. Since in the compressed protein layer the concentration is larger, a larger refractive index (1.49) has been used in a second fit.

Moreover, as the secondary structure does not considerably change neither during adsorption nor during compression, the tertiary structure of the protein could be affected upon adsorption and contribute to a lower interfacial film thickness compared to the dimensions of the molecule in bulk solution. Comparison of the RA intensities in equilibrium to the ones after compression shows a clear increase in the RA intensity of the OH band (see Fig. 12).

Fig. 13 shows the AFM images with a scratch of the film in equilibrium and after compression to 30 mN/m. Comparable to Fig. 10, the images display a coherent film containing some areas of increased height representing agglomerated protein material

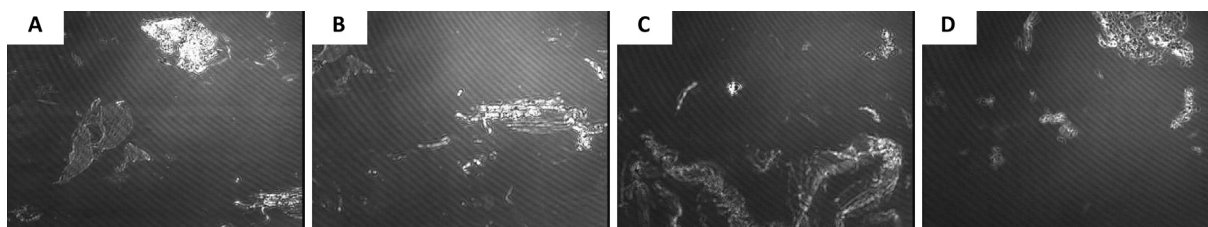


Fig. 9. BAM images of IgG during adsorption (A: $\pi = 6.2$ mN/m, B: $\pi = 18.5$ mN/m) and compression (C: $\pi = 25.0$ mN/m, D: $\pi = 35.0$ mN/m).

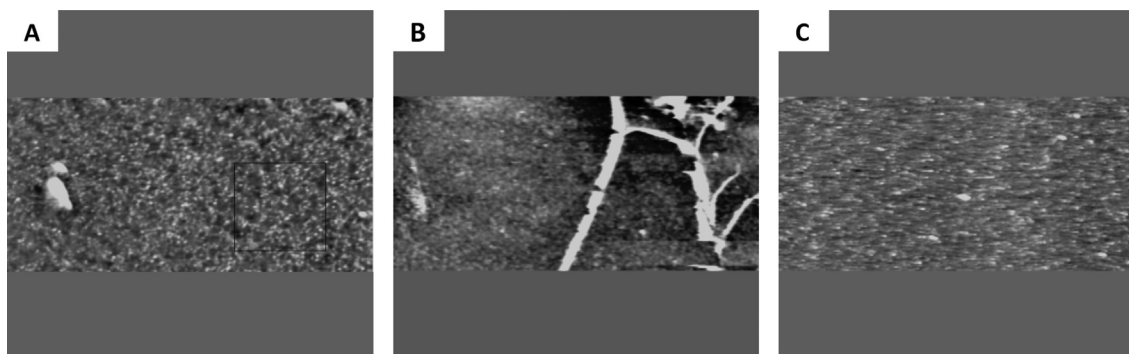


Fig. 10. Underwater AFM images in tapping mode (image size: $10 \times 10 \mu\text{m}^2$) of IgG after adsorption to equilibrium surface pressure (A: 18.5 mN/m), compression (B: 30 mN/m) and after decompression of the film.

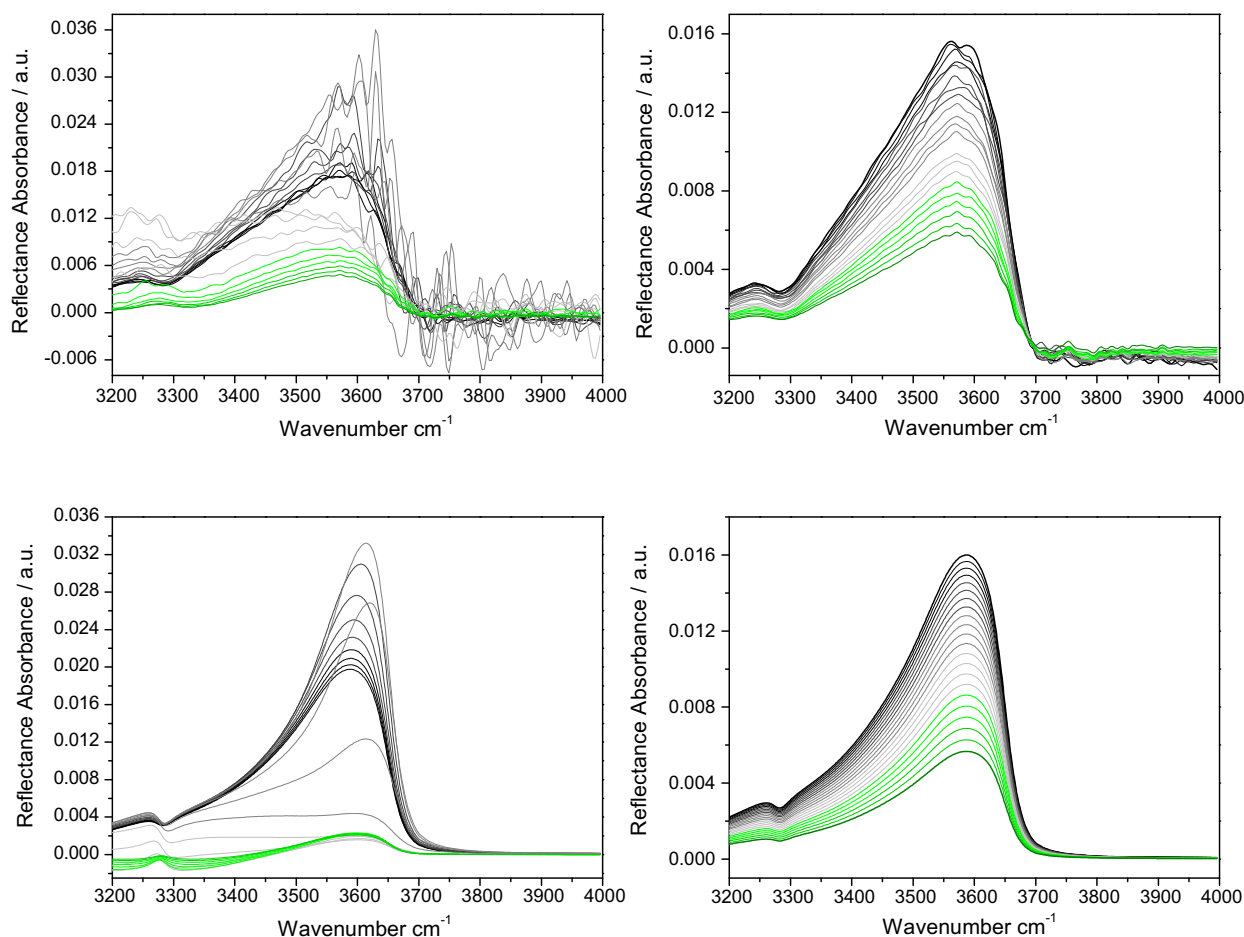


Fig. 11. IRRAS spectra of the OH-stretching vibration and the amide A band of IgG in equilibrium at 18.5 mN/m at different angles of incidence (AoI) from 30° to 72° (from black via grey to green) in steps of 2° , top: experimental spectra (left: p-polarized light, right: s-polarized light), bottom: the corresponding simulated IRRAS spectra.

(Fig. 13A + B). Compression caused wrinkling and the formation of a telescoped protein film (Fig. 13C + D). Section analysis of the AFM height measurements resulted in a mean film thickness of (6.41 ± 2.05) nm in equilibrium and of (5.56 ± 2.94) nm after compression.

4. Summary & conclusions

The use of a Langmuir film balance in combination with IRRAS, BAM and AFM is a novel approach for the characterization of films formed by protein biopharmaceuticals at the liquid–air interface.

The IgG investigated in this study shows a pronounced amphiphilic behavior. It adsorbs to the liquid–air interface in a time- and concentration-dependent manner, reaching a maximum equilibrium adsorption pressure after about 4 hours at concentrations ≥ 1 mg/mL. An additional concentration dependent measurement series indicated that identical equilibrium surface pressure values were reached at concentrations of 1 mg/mL IgG and above (Fig. 1b).

Adsorption of the IgG results in the formation of a highly viscous protein film wherein the protein covers the entire interface, while showing an inhomogeneous distribution as demonstrated by BAM and AFM. The overall increased brightness in BAM images

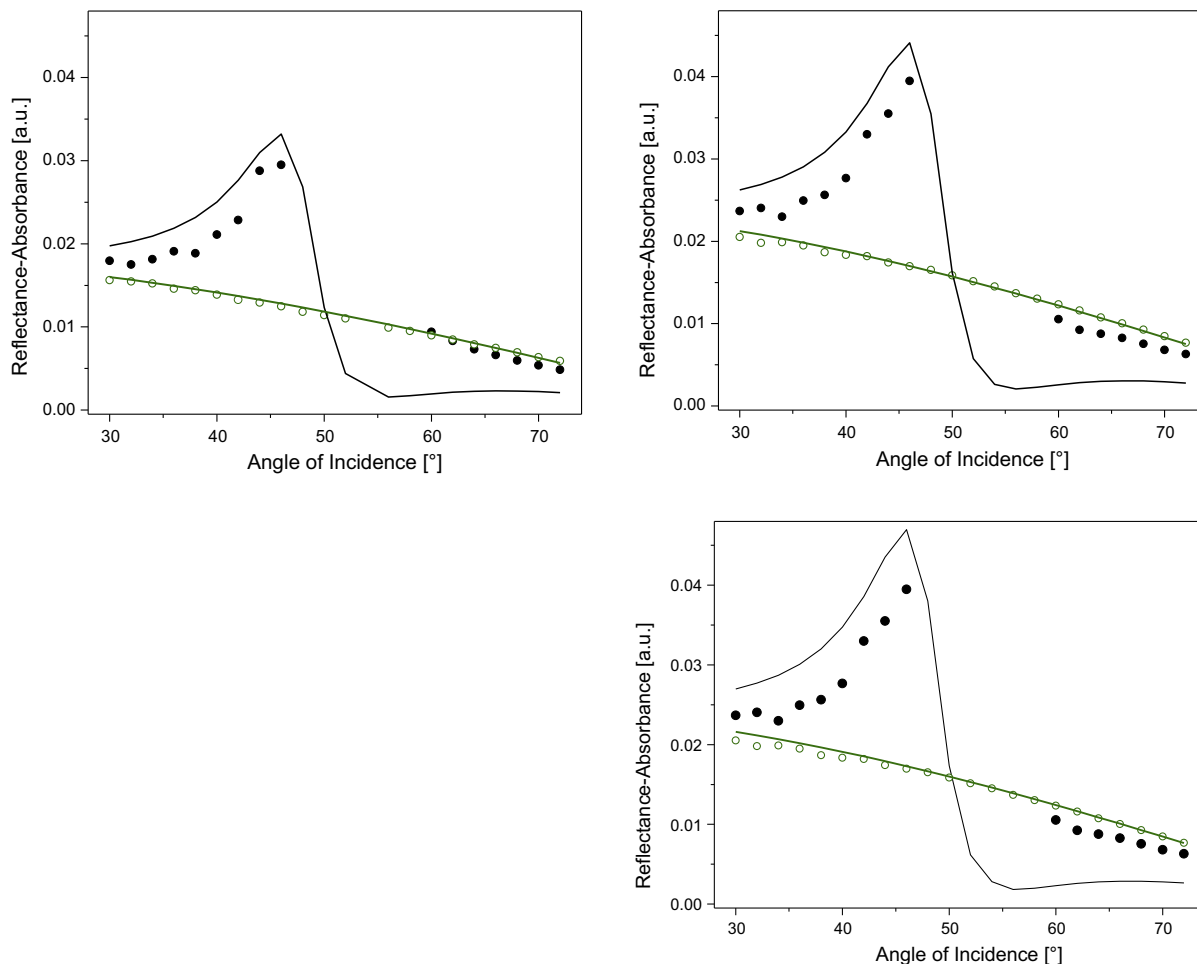


Fig. 12. Experimental (dots) and simulated (solid lines) RA intensities using p-polarized (black) and s-polarized (green) light at the maximum position of the OH-stretching vibration. Top left: data obtained at the equilibrium surface pressure, top right: data after compression to 30 mN/m. Top row: a refractive index of 1.45 has been taken for the equilibrium as well as for the compressed layer. Bottom row: An increased refractive index of 1.49 has been taken for the compressed film.

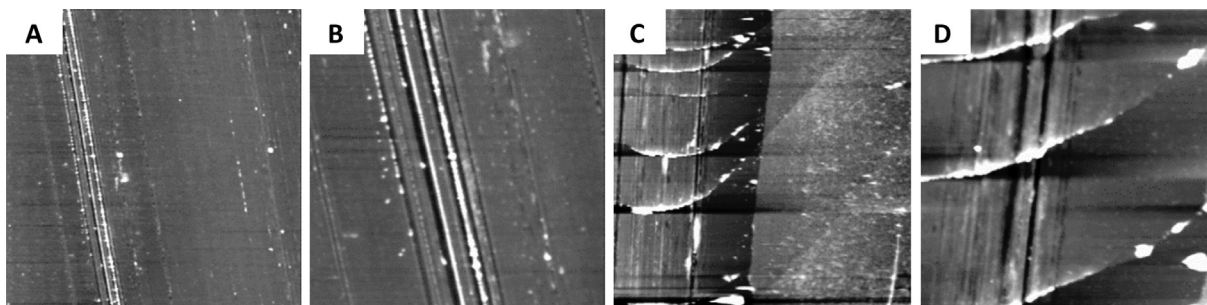


Fig. 13. Underwater AFM images incl. scratch for determination of film thickness in tapping mode (image size: A + C: $30 \times 30 \mu\text{m}^2$, B + D: $10 \times 10 \mu\text{m}^2$) of IgG after adsorption to equilibrium surface pressure (A and B: 18.5 mN/m) and after compression (C and D: 30 mN/m).

can be attributed to the presence of the protein film at the interface. The presence of island structures is related to the inhomogeneous IgG adsorption by forming areas of increased thickness or packing density [27,59]. After adsorption, AFM images reveal a continuous protein film with island structures of condensed protein material similar to BAM but on a smaller scale. The appearance of the OH-vibrational band and amide bands in the IRR spectra substantiate the presence of the protein at the interface

[41,74,75]. Therefore, the accumulation of IgG at the interface was demonstrated by the different methods.

Compression of the film causes a considerable increase in surface pressure above equilibrium values. Not only during adsorption, but all the more upon compression the intensity of the IRR bands increases. This signifies an increase in interfacial film density and thickness [43,76,77]. The orientation of the IgG molecules does not change during adsorption or compression as the dichroic

ratio does not change with increasing surface pressure. As the dichroic ratio was recorded at different surface pressures during adsorption as well as during compression, possible changes, e.g. in telescoped regions of the compressed film, are considered on average.

During compression, the appearance of the BAM images does not change. In contrast, the AFM images reveal substantial changes of the film topography upon compression. The appearance of telescoped protein material with an increased height compared to the adsorbed film evince that the interfacial film is directly affected by compressive forces [33,73]. Hence, the protein tends to be trapped at the interface and does not readily desorb upon compression [78] but forms instead protuberances if the packing density is too high. As secondary structure and molecule orientation were not considerably affected neither by adsorption nor compression, changes in the tertiary structure of the protein could be causative for the compressibility of the interfacial film and the related impeded desorption of protein molecules from the interface.

The IRRAS spectra enable not only conclusions about the presence and film thickness of the IgG at the interface, but also about the protein secondary structure elements. For different types of proteins unfolding upon adsorption to the liquid–air interface has been reported [25,72,79,80]. In contrast to this, our results do not indicate considerable changes in the secondary structure of IgG after adsorption and compression. This can be explained by the fact that IgG molecules belong to the most stable protein types [65,81]. As no new structural elements show up compared to the native secondary structure in solution the IgG remains in a native-like secondary structure. According to literature, IR methods cover changes of ≥ 2 –10% in sensitivity [70,82]. Minor structural perturbations, however, are not detected and cannot be excluded.

The interfacial film thickness was determined from the analysis of the IRRAS intensity of the OH-stretching band as a function of angle of incidence. At equilibrium adsorption pressure (18.5 mN/m), the film thickness amounts to 1.97 nm ($n = 1.45$), and compression to 30mN/m caused an increase in film thickness to 2.61 nm assuming the same refractive index of 1.45 or to 2.4 assuming a higher refractive index of 1.49 for the compressed layer. These values are clearly smaller compared with the ones determined by AFM for the equilibrium film, but in good agreement with the AFM results of the compressed film. The fact, that the calculated film thickness (1.97 nm) is only 30% of the hydrodynamic radius of the molecule (6.9 nm) can be explained by the loose packing in the equilibrium film. This film contains a substantial amount of water. Algorithms have been devised for estimating the amount of bound water from the amino acid sequence, although these generally do not distinguish between exposed and buried residues. The first ones bind water and the second ones do not. This substantial amount of water in the protein layer leads to the underestimation of the film thickness by IRRAS using the experimentally determined OH-band. Therefore, the thickness of the transferred film determined by AFM is closer to the value of the hydrodynamic radius. On the other hand, it has been stated that IgG molecules preferentially adsorb in flat orientations, which can explain reduced interfacial film thicknesses compared to the values of hydrodynamic radius measured in solution [83,84]. Erickson [85] determined the minimal radius of a sphere that could contain a protein with 100 kDa to 3.05 nm and for 200 kDa to 3.84 nm. Additionally, they stated the average separation of molecules (center to center) to be 6.9 nm [85]. If the film is compressed to 30 mN/m, some water will be squeezed out and the protein film might change to be flatter. Therefore, the thickness of this more densely packed film determined by IRRAS is in good agreement with the value determined by AFM. Although the optical properties could only be estimated from values measured in bulk solution, a quali-

tative statement on the change in film thickness (packing density) and a differentiation between the film thickness at equilibrium adsorption pressure and after compression can be clearly made.

Compression-decompression cycles reveal compressibility of the protein film [33,73,86] indicating a non-equilibrium state of the adsorption layer and therefore drastically reduced desorption kinetics. The considerable hysteresis indicates physical changes within the film as the packing density and film thickness change with compression and decompression. Furthermore, each subsequent cycle ended up in slightly lower surface pressures indicating a loss of material from the interface which is in accordance with the morphology of the protein film exhibiting protrusions after compression. These areas of protein material which are formed by compression and visualized by AFM are no longer present after decompression. Decompression results in a smoother surface compared to adsorption or compression indicated by a decrease in the mean roughness of the film. The decrease in mean roughness also substantiates the assumption for partial loss of material from the interface and compaction of the film by reorganization of the protein molecules, what is in agreement with the results obtained by the surface pressure measurements [33,34,73,87,88].

Altogether, the combination of physical–chemical, spectroscopic, and microscopic methods for surface characterization provides useful insights into the behavior of proteins at the liquid–air interface. Further investigations will show what impact not only the IgG itself, but also different formulation parameters such as pH and the presence of additives have on the liquid–air interfacial behavior and the tendency of an antibody to aggregate as a measure of protein stability. Moreover, it has already been shown that continuous compression and decompression of an interfacial protein film causes compaction followed by aggregation [33,73]. Thus physical changes within the protein film can be causative for liquid–air interface-related protein aggregation [33,89].

In conclusion, during adsorption to the soft liquid–air interface IgG forms a continuous but inhomogeneous film of native-like protein molecules whose topographical appearance is affected by compressive forces. As protein pharmaceuticals are exposed to liquid–air interfaces at many points during development, production and storage [90], this comprehensive understanding of the underlying mechanisms is of great importance, as it can help to improve protein stability by choosing appropriate formulation, processing and packing conditions [91,92].

Acknowledgements

This work was supported by AbbVie Deutschland GmbH & Co. KG, Ludwigshafen am Rhein, Germany.

Special thanks go to Irina Berndt and Anneliese Heilig (MPI-KGF Potsdam) for technical support.

References

- [1] J.K.H. Liu, The history of monoclonal antibody development - Progress, remaining challenges and future innovations, 3 (2014) 113–116.
- [2] N. Rathore, R.S. Rajan, Current perspectives on stability of protein drug products during formulation, fill and finish operations, *Biotechnol. Prog.* 24 (3) (2008) 504–514.
- [3] A.S. Rosenberg, Effects of protein aggregates: an immunologic perspective, *AAPS J.* 8 (3) (2006) E501–E507.
- [4] W. Wang, S.K. Singh, N. Li, M.R. Toler, K.R. King, S. Nema, Immunogenicity of protein aggregates—concerns and realities, *Int. J. Pharm.* 431 (1–2) (2012) 1–11.
- [5] E.M. Moussa, J.P. Panchal, B.S. Moorthy, J.S. Blum, M.K. Joubert, L.O. Narhi, E.M. Topp, Immunogenicity of therapeutic protein aggregates, *J. Pharm. Sci.* 105 (2) (2016) 417–430.
- [6] W. Jiskoot, T.W. Randolph, D.B. Volkin, C.R. Middaugh, C. Schöneich, G. Winter, W. Friess, D.J.A. Crommelin, J.F. Carpenter, Protein instability and immunogenicity: roadblocks to clinical application of injectable protein delivery systems for sustained release, *J. Pharm. Sci.* 101 (3) (2012) 946–954.
- [7] C.J. Roberts, Protein aggregation and its impact on product quality, *Curr. Opin. Biotechnol.* 30 (2014) 211–217.

- [8] R. Lumry, H. Eyring, Conformational changes of proteins, *J. Phys. Chem* 58 (2) (1954) 110–120.
- [9] Y. Li, C.J. Roberts, Lumry-Eyring nucleated-polymerization model of protein aggregation kinetics, *J. Phys. Chem. B* 113 (19) (2009) 7020–7032.
- [10] E. Chi, S. Krishnan, B.S. Kendrick, B.S. Chang, J.F. Carpenter, T.W. Randolph, Roles of conformational stability and colloidal stability in the aggregation of recombinant human granulocyte colony-stimulating factor, *Protein Sci.* 12 (2003) 903–913.
- [11] C. J. Roberts, "Kinetics of Irreversible Protein Aggregation: Analysis of Extended Lumry - Eyring Models and Implications for Predicting Protein Shelf Life," pp. 1194–1207, 2003.
- [12] R.J. Green, I. Hopkinson, R.A.L. Jones, Unfolding and intermolecular association in globular proteins adsorbed at interfaces, *Langmuir* 15 (6) (1999) 5102–5110.
- [13] L.R. De Young, A.L. Fink, K.A. Dills, Aggregation of globular proteins, *Acc. Chem. Res.* 26 (15) (1993) 614–620.
- [14] R. Wetzel, Mutations and off-pathway aggregation of proteins, *Trends Biotechnol.* 12 (5) (1994) 193–198.
- [15] J.S. Philo, T. Arakawa, Mechanisms of protein aggregation, *Curr. Pharm. Biotechnol.* 10 (2009) 348–351.
- [16] W. Wang, S. Nema, D. Teagarden, Protein aggregation - pathways and influencing factors, *Int. J. Pharm.* 390 (2) (2010) 89–99.
- [17] S. Zorrilla, G. Rivas, A.U. Acuna, M.P. Lillo, Protein self-association in crowded protein solutions: a time-resolved fluorescence polarization study, *Protein Sci.* 13 (11) (2004) 2960–2969.
- [18] S. Damodaran, L. Razumovsky, Role of surface area-to-volume ratio in protein adsorption at the air-water interface, *Surf. Sci.* 602 (1) (2008) 307–315.
- [19] M. Rodriguezno, C. Sanchez, V. Ruizhenestrosa, J. Patino, Milk and soy protein films at the air-water interface, *Food Hydrocoll.* 19 (3) (2005) 417–428.
- [20] J.M.R. Patino, S.E.M. Ortíz, C.C. Sánchez, R.R. Niño, C. Anon, Behavior of soy globulin films at the air-water interface. *Struct. Dilatation. Properties Spread Films* 68 (2005) 429–437.
- [21] P. Parhi, A. Golas, N. Barnthip, H. Noh, E.A. Vogler, Volumetric interpretation of protein adsorption: capacity scaling with adsorbate molecular weight and adsorbent surface energy, *Biomaterials* 30 (36) (2009) 6814–6824.
- [22] A. Krishnan, C.A. Siedlecki, E.A. Vogler, Traube-rule interpretation of protein adsorption at the liquid - vapor interface, (12) (2003) 10342–10352.
- [23] E.A. Vogler, Protein adsorption in three dimensions, *Biomaterials* 33 (5) (2012) 1201–1237.
- [24] M. Rabe, D. Verdes, S. Seeger, Understanding protein adsorption phenomena at solid surfaces, *Adv. Colloid Interface Sci.* 162 (1–2) (2011) 87–106.
- [25] Y.F. Yano, Kinetics of protein unfolding at interfaces, *J. Physics. Condens. Matter* 24 (2012) 503101.
- [26] J.S. Bee, T.W. Randolph, J.F. Carpenter, S.M. Bishop, M.N. Dimitrova, Review: Effects of surfaces and leachables on the stability of biopharmaceuticals, *J. Pharm. Sci.* 100 (10) (2011) 4158–4170.
- [27] P. Wilde, A. Mackie, F. Husband, P. Gunning, V. Morris, Proteins and emulsifiers at liquid interfaces, *Adv. Colloid Interface Sci.* 108–109 (2004) 63–71.
- [28] R. Thirumangalathu, S. Krishnan, M. Ricci, N. Brems, T.W. Randolph, J.F. Carpenter, Silicone oil- and agitation-induced aggregation of a monoclonal antibody in aqueous solution, *J. Pharm. Sci.* 98 (9) (2009).
- [29] V. Saller, J. Matilainen, U. Grauschopf, K. Bechtold-Peters, H.-C. Mahler, W. Friess, Particle shedding from peristaltic pump tubing in biopharmaceutical drug product manufacturing, *J. Pharm. Sci.* 104 (4) (2015) 1440–1450.
- [30] A. Eppler, M. Weigandt, A. Hanefeld, H. Bunjes, Relevant shaking stress conditions for antibody preformulation development, *Eur. J. Pharm. Biopharm.* 74 (2) (2010) 139–147.
- [31] H.C. Mahler, R. Müller, W. Frieß, A. Delille, S. Matheus, Induction and analysis of aggregates in a liquid IgG1-antibody formulation, *Eur. J. Pharm. Biopharm.* 59 (2005) 407–417.
- [32] S. Kiese, A. Pappenberger, W. Friess, H.-C. Mahler, Shaken, not stirred: mechanical stress testing of an IgG1 antibody, *J. Pharm. Sci.* 97 (10) (2008) 4337–4366.
- [33] J.S. Bee, D.K. Schwartz, S. Trabelsi, E. Freund, J.L. Stevenson, J.F. Carpenter, T.W. Randolph, Production of particles of therapeutic proteins at the air-water interface during compression/dilation cycles, *Soft Matter* 8 (2012) 10329.
- [34] S. Rudiuk, L. Cohen-Tannoudji, S. Huille, C. Tribet, Importance of the dynamics of adsorption and of a transient interfacial stress on the formation of aggregates of IgG antibodies, *Soft Matter* 8 (9) (2012) 2651.
- [35] H.J. Lee, A. McAuley, K.F. Schilke, J. McGuire, Molecular origins of surfactant-mediated stabilization of protein drugs, *Adv. Drug Deliv. Rev.* 63 (13) (2011) 1160–1171.
- [36] T. Serno, E. Härtl, A. Besheer, R. Miller, G. Winter, The role of polysorbate 80 and HPβCD at the air-water interface of IgG solutions, *Pharm. Res.* (2012) 1–14.
- [37] A. Hawe, W. Friess, Formulation development for hydrophobic therapeutic proteins, *Pharm. Dev. Technol.* 12 (October) (2007) 223–237.
- [38] B.A. Kerwin, Polysorbates 20 and 80 used in the formulation of protein biotherapeutics: structure and degradation pathways, *J. Pharm. Sci.* 97 (8) (2008) 2926–2935.
- [39] A. Savitzky, M.J.E. Golay, Smoothing and differentiation of data by simplified least squares procedures, *Anal. Chem.* 36 (8) (1964) 1627–1639.
- [40] R. Mendelsohn, External infrared reflection absorption spectrometry of monolayer films at the air-water interface, *Annu. Rev. Phys. Chem.* 46 (1995) 305–334.
- [41] C.R. Flach, J.W. Brauner, J.W. Taylor, R.C. Baldwin, R. Mendelsohn, External reflection FTIR of peptide monolayer films in situ at the air/water interface: experimental design, spectra-structure correlations, and effects of hydrogen-deuterium exchange, *Biophys. J.* 67 (1) (1994) 402–410.
- [42] A.H. Muentzer, J. Hentschel, H.G. Borner, G. Brezesinski, Characterization of peptide-guided polymer assembly at the air/water interface, *Langmuir* 24 (7) (2008) 3306–3316.
- [43] C. Schwieger, B. Chen, C. Tschierske, J. Kressler, A. Blume, Organization of T-shaped facial amphiphiles at the air/water interface studied by infrared reflection absorption spectroscopy, *J. Phys. Chem. B* 116 (40) (2012) 12245–12256.
- [44] S. Schrettli, C. Stefanu, C. Schwieger, G. Pasche, E. Oveisi, Y. Fontana, A. Fontcuberta i Morral, J. Reguera, R. Petraglia, C. Corminboeuf, G. Brezesinski, H. Frauenrath, Functional carbon nanosheets prepared from hexayne amphiphile monolayers at room temperature, *Nat. Chem.* 6 (6) (2014) 468–476.
- [45] V.L. Kuzmin, A.V. Mikhailov, Molecular theory of light reflection and applicability limits of the macroscopic approach, *Opt. Spectrosc.* 51 (4) (1981) 383–385.
- [46] V.L. Kuzmin, V.P. Romanov, A.V. Mikhailov, Reflection of light at the boundary of liquid systems and structure of the surface layer: a review, *Opt. Spectrosc.* 73 (1) (1992) 1–26.
- [47] J.E. Bertie, Z. Lan, Infrared intensities of liquids XX: The intensity of the OH stretching band of liquid water revisited, and the best current values of the optical constants of H₂O(l) at 25 °C between 15,000 and 1 cm⁻¹, *Appl. Spectrosc.* 50 (8) (1996) 1047–1057.
- [48] J.E. Bertie, M.K. Ahmed, H.H. Eysel, Infrared Intensities of Liquids. 5. Optical and dielectric constants, integrated intensities, and dipole moment derivatives of H₂O and D₂O at 22 °C, *J. Phys. Chem.* 93 (1989) 2210–2218.
- [49] E. Maltseva, A. Kerth, A. Blume, H. Möhwald, G. Brezesinski, Adsorption of amyloid β (1–40) peptide at phospholipid monolayers, *ChemBioChem* 6 (10) (2005) 1817–1824.
- [50] E. Amado, A. Kerth, A. Blume, J. Kressler, Infrared reflection absorption spectroscopy coupled with brewster angle microscopy for studying interactions of amphiphilic triblock copolymers with phospholipid monolayers, *Langmuir* 24 (18) (2008) 10041–10053.
- [51] A. Kerth, A. Erbe, M. Dathe, A. Blume, Infrared reflection absorption spectroscopy of amphipathic model peptides at the air/water interface, *Biophys. J.* 86 (6) (2004) 3750–3758.
- [52] A. Meister, C. Nicolini, H. Waldmann, J. Kuhlmann, A. Kerth, R. Winter, A. Blume, Insertion of lipidated Ras proteins into lipid monolayers studied by infrared reflection absorption spectroscopy (IRRAS), *Biophys. J.* 91 (4) (2006) 1388–1401.
- [53] S. Hénon, J. Meunier, Microscope at the Brewster angle: direct observation of first-order phase transitions in monolayers, *Rev. Sci. Instrum.* 62 (4) (1991) 936–939.
- [54] D. Hoening, D. Moebius, Direct visualization of monolayers at the air-water interface by Brewster angle microscopy, *J. Phys. Chem.* 2 (1991) 4590–4592.
- [55] D. Vollhardt, Brewster angle microscopy: a preferential method for mesoscopic characterization of monolayers at the air/water interface, *Curr. Opin. Colloid Interface Sci.* 19 (3) (2014) 183–197.
- [56] B.C. Tripp, J.J. Magda, J.D. Andrade, Adsorption of globular proteins at the air/water interface as measured via dynamic surface tension, *J. Colloid Interface Sci.* 173 (1) (1995) 16–27.
- [57] H.L. Kim, A. McAuley, B. Livesay, W.D. Gray, J. McGuire, Modulation of protein adsorption by poloxamer 188 in relation to polysorbates 80 and 20 at solid surfaces, *J. Pharm. Sci.* 103 (4) (2014) 1043–1049.
- [58] D.E. Graham, M.C. Phillips, Proteins at liquid Interfaces - III. Molecular structures of adsorbed films, *J. Colloid Interface Sci.* 70 (3) (1979) 427–439.
- [59] R.R. Niño, C.C. Sánchez, V.P. Ruiz-Henestrosa, J.M.R. Patino, Milk and soy protein films at the air-water interface, *Food Hydrocoll.* 19 (3) (2005) 417–428.
- [60] J.M.R. Patino, S.E.M. Ortíz, C.C. Sánchez, R.R. Niño, C. Anon, Behavior of soy globulin films at the air-water interface. structural and dilatational properties of spread films, *Ind. Eng. Chem. Res.* 42 (21) (2003) 5011–5017.
- [61] R.R. Niño, C.C. Sánchez, J.M.R. Patino, Interfacial characteristics of β-casein spread films at the air-water interface, *Colloids Surfaces B Biointerfaces* 12 (3–6) (1999) 161–173.
- [62] J.M.R. Patino, C.C. Sánchez, M.R. Niño, Structural and morphological characteristics of β-casein monolayers at the air-water interface, *Food Hydrocoll.* 13 (5) (1999) 401–408.
- [63] I.S. Chronakis, A.N. Galatanu, T. Nylander, B. Lindman, The behaviour of protein preparations from blue-green algae (*Spirulina platensis* strain Pacifica) at the air/water interface, *Colloids Surfaces A Physicochem. Eng. Asp.* 173 (1–3) (2000) 181–192.
- [64] T. Menzen, W. Friess, Temperature-ramped studies on the aggregation, unfolding, and interaction of a therapeutic monoclonal antibody, *J. Pharm. Sci.* 103 (2) (2014) 445–455.
- [65] S. Matheus, W. Friess, H.C. Mahler, FTIR and nDSC as analytical tools for high-concentration protein formulations, *Pharm. Res.* 23 (6) (2006) 1350–1363.
- [66] N. Takeda, M. Kato, Y. Taniguchi, Pressure- and thermally-induced reversible changes in the secondary structure of ribonuclease A studied by FT-IR spectroscopy, *Biochemistry* 34 (17) (1995) 5980–5987.
- [67] S. Krimm, J. Bandekar, Vibrational spectroscopy and conformation of peptides, polypeptides, and proteins, *Adv. Protein Chem.* 38 (1986) 181–364.
- [68] A. Meister, A. Kerth, A. Blume, Interaction of sodium dodecyl sulfate with dimyristoyl-sn-glycero-3-phosphocholine monolayers studied by infrared

- reflection absorption spectroscopy. A new method for the determination of surface partition coefficients, *J. Phys. Chem. B* 108 (24) (2004) 8371–8378.
- [69] V.S. Alahverdijeva, K. Khristov, D. Exerowa, R. Miller, Correlation between adsorption isotherms, thin liquid films and foam properties of protein/surfactant mixtures: Lysozyme/C10DMPO and lysozyme/SDS, *Colloids Surfaces A Physicochem. Eng. Asp.* 323 (1–3) (2008) 132–138.
- [70] J. Kong, S. Yu, Fourier transform infrared spectroscopic analysis of protein secondary structures, *Acta Biochim. Biophys. Sin. (Shanghai)* 39 (8) (2007) 549–559.
- [71] F.F.O. Sousa, A. Luzardo-Álvarez, J. Blanco-Méndez, F.J. Otero-Espinar, M. Martín-Pastor, I. Sández Macho, Use of ¹H NMR STD, WaterLOGSY, and Langmuir monolayer techniques for characterization of drug-zein protein complexes, *Eur. J. Pharm. Biopharm.* 85 (3) (2013) 790–798.
- [72] T. Furuno, Atomic force microscopy study on the unfolding of globular proteins in the Langmuir films, *Thin Solid Films* 552 (2014) 170–179.
- [73] S. Ghazvini, C. Kalonia, D.B. Volkin, P. Dhar, Evaluating the role of the air–solution interface on the mechanism of subvisible particle formation caused by mechanical agitation for an IgG1 mAb, *J. Pharm. Sci.* 105 (5) (2016) 1643–1656.
- [74] S.Y. McLoughlin, M. Kastantin, D.K. Schwartz, J.L. Kaar, Single-molecule resolution of protein structure and interfacial dynamics on biomaterial surfaces, *Proc. Natl. Acad. Sci. U.S.A.* 110 (2013) 19396–19401.
- [75] R. Mendelsohn, G. Mao, C.R. Flach, Infrared reflection-absorption spectroscopy: principles and applications to lipid–protein interaction in Langmuir films, *Biochim. Biophys. Acta - Biomembr.* 1798 (4) (2010) 788–800.
- [76] M. Hoernke, J.A. Falenski, C. Schwieger, B. Koksche, G. Brezesinski, Triggers for β -sheet formation at the hydrophobic–hydrophilic interface: high concentration, in-plane orientational order, and metal ion complexation, *Langmuir* 27 (2011) 14218–14231.
- [77] C. Stefaniu, G. Brezesinski, H. Möhwald, Langmuir monolayers as models to study processes at membrane surfaces, *Adv. Colloid Interface Sci.* 208 (2014) 197–213.
- [78] L. Wang, D. Atkinson, D.M. Small, Interfacial properties of an amphipathic α -helix consensus peptide of exchangeable apolipoproteins at air/water and oil/water interfaces, *J. Biol. Chem.* 278 (39) (2003) 37480–37491.
- [79] Y.F. Yano, E. Arakawa, W. Voegeli, T. Matsushita, Real-time investigation of protein unfolding at an air–water interface at the 1 s time scale, *J. Synchrotron Radiat.* 20 (6) (2013) 980–983.
- [80] P. Pal, T. Kamilya, M. Mahato, G.B. Talapatra, The formation of pepsin monomolecular layer by the Langmuir–Blodgett film deposition technique, *Colloids Surfaces B Biointerfaces* 73 (2009) 122–131.
- [81] M.J. Feige, L.M. Hendershot, J. Buchner, How antibodies fold, *Trends Biochem. Sci.* 35 (4) (2010) 189–198.
- [82] M. Jackson, H.H. Mantsch, The use and misuse of FTIR spectroscopy in the determination of protein structure, *Crit. Rev. Biochem. Mol. Biol.* 30 (2) (1995) 95–120.
- [83] R. Saber, S. Sarkar, P. Gill, B. Nazari, F. Faridani, High resolution imaging of IgG and IgM molecules by scanning tunneling microscopy in air condition, *Sci. Iran.* 18 (6) (2011) 1643–1646.
- [84] J.G. Vilhena, A.C. Dumitru, E.T. Herruzo, J.I. Mendieta-Moreno, R. Garcia, P.A. Serena, R. Pérez, Adsorption orientations and immunological recognition of antibodies on graphene, *Nanoscale* (2016) 13463–13475.
- [85] H.P. Erickson, Size and shape of protein molecules at the nanometer level determined by sedimentation, gel filtration, and electron microscopy, *Biol. Proced. Online* 11 (1) (2009) 32–51.
- [86] R.G. Couston, D.A. Lamprou, S. Uddin, C.F. Van Der Walle, Interaction and destabilization of a monoclonal antibody and albumin to surfaces of varying functionality and hydrophobicity, *Int. J. Pharm.* 438 (1–2) (2012) 71–80.
- [87] P.A. Wierenga, H. Gruppen, New views on foams from protein solutions, *Curr. Opin. Colloid Interface Sci.* 15 (5) (2010) 365–373.
- [88] M. Nieto-Suárez, N. Vila-Romeu, I. Prieto, Behaviour of insulin Langmuir monolayers at the air–water interface under various conditions, *Thin Solid Films* 516 (24) (2008) 8873–8879.
- [89] I.C. Shieh, A.R. Patel, Predicting the agitation-induced aggregation of monoclonal antibodies using surface tensiometry, *Mol. Pharm.* 3184–3193 (2015).
- [90] J.S. Bee, J.L. Stevenson, B. Mehta, J. Svitel, J. Pollastrini, R. Platz, E. Freund, J.F. Carpenter, T.W. Randolph, Response of a concentrated monoclonal antibody formulation to high shear, *Biotechnol. Bioeng.* 103 (5) (2009) 936–943.
- [91] N.A. Alexandrov, K.G. Marianova, T.D. Gurkov, K.D. Danov, P.A. Kralchevsky, S. D. Stoyanov, T.B. Blijdenstein, I.N. Arnaudov, E.G. Pelan, A. Lips, Interfacial layers from the protein HFBII hydrophobin: dynamic surface tension, dilatational elasticity and relaxation times, *J. Colloid Interface Sci.* 376 (1) (2012) 296–306.
- [92] C.J. Roberts, T.K. Das, E. Sahin, Predicting solution aggregation rates for therapeutic proteins: approaches and challenges, *Int. J. Pharm.* 418 (2) (2011) 318–333.